ACS APPLIED MATERIALS & INTERFACES

Research Article

Cite This: ACS Appl. Mater. Interfaces 2017, 9, 40187-40196

www.acsami.org

Rapidly Synthesized, Few-Layered Pseudocapacitive SnS_2 Anode for High-Power Sodium Ion Batteries

Ranjith Thangavel,[†] Amaresh Samuthira Pandian,[‡] Hari Vignesh Ramasamy,[†] and Yun-Sung Lee*[,†]

[†]Faculty of Applied Chemical Engineering, Chonnam National University, Gwang-ju 500-757, Korea

[‡]Materials Science and Technology Division, Oak Ridge National Laboratory, Oak Ridge, Tennessee 37831, United States

Supporting Information

ABSTRACT: The abundance of sodium resources has recently motivated the investigation of sodium ion batteries (SIBs) as an alternative to commercial lithium ion batteries. However, the low power and low capacity of conventional sodium anodes hinder their practical realization. Although most research has concentrated on the development of high-capacity sodium anodes, anodes with a combination of high power and high capacity have not been widely realized. Herein, we present a simple microwave irradiation technique for obtaining few-layered, ultrathin two-dimensional SnS_2 over graphene sheets in a few minutes. SnS_2 possesses a large number of active surface sites and exhibits high-capacity, rapid sodium ion storage kinetics induced by quick, nondestructive pseudocapacitance. Enhanced sodium ion storage at a high current density (12 A g^{-1}), accompanied by high reversibility and high stability, was demonstrated. Additionally, a rationally designed sodium ion full cell coupled with $SnS_2//Na_3V_2(PO_4)_3$ exhibited exceptional performance with high initial Coulombic efficiency (99%), high capacity, high stability, and a retention of ~53% of the initial capacity even after the current density was increased by a factor of 140. In addition, a high specific energy of ~140 Wh kg^{-1} and an ultrahigh specific power of ~8.3 kW kg^{-1} (based on the mass of both the anode and cathode) were observed. Because of its outstanding performance and rapid synthesis, few-layered SnS_2 could be a promising candidate for practical realization of high-power SIBs.

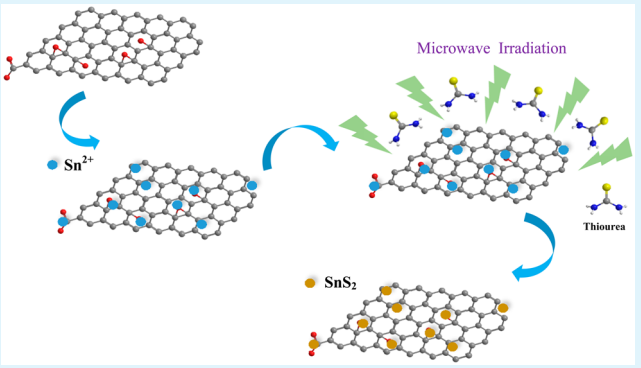

KEYWORDS: *sodium ion battery, SnS_2, anode, high power, energy storage*

INTRODUCTION

Attempts to develop high-performance sodium ion batteries (SIBs) with characteristics equivalent to those of lithium ion batteries (LIBs) have been the focus of increasing attention in recent years.[1,2] Owing to the natural abundance of sodium resources and the similar working chemistry and energy density of LIBs, SIBs are an appealing and low-cost candidate for large-scale smart grid applications.[3,4] As a result of ongoing research on cathode materials for SIBs, a variety of layered oxides, phosphates, and fluorides with high capacity and high rate properties have been identified.[5−8]

However, developing high-capacity anode materials for adoption in commercial SIBs remains challenging.[7,9] Although graphite anodes have been successfully applied in commercial LIBs, they do not support the intercalation reaction with Na^+ ions. Many amorphous carbon materials such as hard carbon, carbon sheets, carbon quantum dots, and nanostructured carbon have been studied as alternative anode materials for SIBs.[10−13] Unfortunately, high-energy-density SIBs cannot be realized using these materials owing to the poor specific capacity of carbonaceous anodes.[12] Despite their high theoretical capacity, many metal oxide anodes showed inferior reversible capacity resulting from poor sodium ion kinetics.[14−16] Metals and metal sulfides have attracted considerable attention for the development of high-energy-density SIBs.[17] Among several studied anodes, layered SnS_2 with a two-dimensional (2D) structure is highly interesting owing to its high reversible discharge capacity, which makes it promising for use in high-energy SIBs. A large interlamellar spacing (0.59 nm) and open structure between the layers afford an ideal structural arrangement that provides a short diffusion path for storage of the relatively large sodium ions.[17,18]

High-performance SnS_2 anodes delivering a high specific capacity and longer cycle life have been studied recently.[18] However, the power characteristics of SnS_2 anodes are unsatisfactory, and further development is necessary toward their use as a high-power, high-capacity anode material for SIBs.[19,20] The fundamental problem arises from the sluggish diffusion processes during the alloying and conversion reactions, which lead to a poor output power. Overcoming the sluggish diffusion process by using fast pseudocapacitive storage could be a favorable strategy for achieving high-power

Received: July 26, 2017
Accepted: October 27, 2017
Published: October 27, 2017

DOI: 10.1021/acsami.7b11040
ACS Appl. Mater. Interfaces 2017, 9, 40187−40196

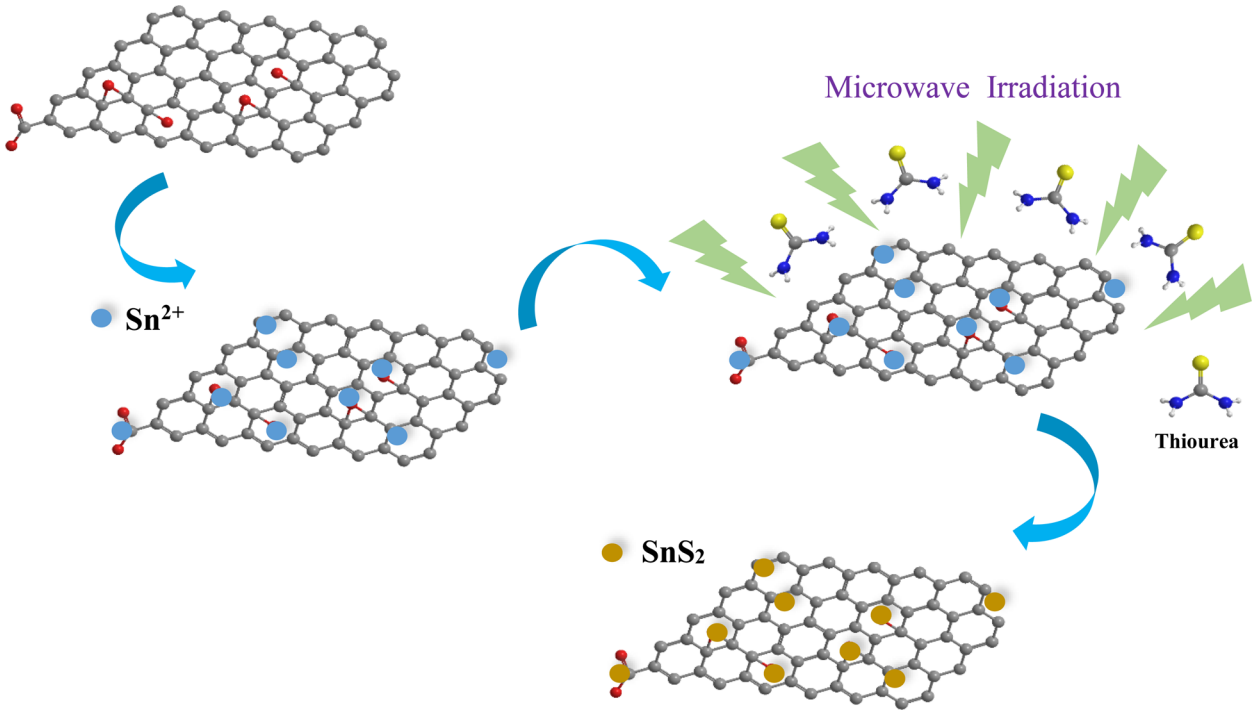

Figure 1. Schematic of synthesis of few-layered SnS_2.

anodes.[21] Although pseudocapacitive charge storage has been realized for metal oxide anodes, pseudocapacitive storage in metal sulfides is still in a nascent stage and needs to be investigated.[15,22] SnS_2, which is an anisotropic crystal with a large interior space, can easily facilitate rapid sodium ion storage.

SnS_2 does not exhibit pseudocapacitive storage in its bulk form. However, highly exfoliated few-layered metal chalcogenides exhibit different chemical and physical properties compared to their bulk counterparts.[23,24] Few-layered SnS_2 can provide a large number of active sites and ion diffusion paths, and the open structure could afford highly favorable fast pseudocapacitive sodium ion storage. The 2D SnS_2 nanoarchitecture embedded in an electrically conductive carbon network could drive fast pseudocapacitive sodium storage, suggesting that a high-power sodium storage system is possible. Mechanical and chemical exfoliation are the most common strategies for preparing highly exfoliated layered metal chalcogenides.[24] However, these techniques are tedious and layered SnS_2 could undergo irreversible chemical and structural modification.[25] Further, the long-duration reaction techniques could result in a stacked structure with large bulky microstructures, hindering the realization of high-power anodes.[26] Exfoliation of layered compounds to thin layers by rapid heating by a microwave technique is currently attracting attention. Furthermore, its simplicity, low cost, and short reaction time, along with the possibility of mass-scale synthesis, makes the microwave technique highly advantageous.[27−29]

Herein, we report ultrafast (a few minutes) microwave synthesis of highly exfoliated few-layered SnS_2 grown over few-layered graphene sheets (SnS_2/G). SnS_2/G was found to be highly mesoporous, and it supported the sodium storage kinetics owing to its short sodium ion diffusion path. The rationally designed SnS_2/G delivered fast sodium ion storage kinetics resulting from surface pseudocapacitive storage behavior and thus shows potential for use as a high-power anode. The tailored architecture provided a large number of active sites and buffered any volume changes during sodium ion insertion; it demonstrates a high capacity and an outstanding rate capability, outperforming conventional metal oxides and carbonaceous sodium anodes.

Our most important finding is that when pseudocapacitive SnS_2 was assembled into a sodium full cell with $Na_3V_2(PO_4)_3$ (NVP), the device performed extremely well, delivering a high specific energy of 140 Wh kg^{-1} and an extremely high specific power of 8.3 kW kg^{-1} (based on the combined mass of the anode and cathode). In addition, outstanding stability for 150 cycles with 85% capacity retention was achieved, and the proposed material offers a promising platform for the development of high-power SIBs for next-generation large-scale energy storage devices.

METHODS

Material Preparation. The starting materials, anhydrous tin(II) chloride anhydrous (99%, Alfa) and thiourea (99%, Sigma-Aldrich) were used as received without further purification. GO was prepared by exfoliation of graphite oxide using a modified Hummers method. In a typical synthesis of the SnS_2/graphene hybrid, GO was well dispersed in a water/ethanol mixture by sonication. The tin salt and thiourea (1:5.3 mol. ratio) was then added to the solution, which was again stirred well. The mixture was then carefully transferred to a microwave oven and exposed to microwave irradiation (Daewoo, 700 W) for 20 min. The resultant product was washed well with water and ethanol several times to remove the residuals and then dried at 90 °C overnight. Pristine SnS_2 was obtained by a similar procedure without the addition of the GO dispersion. The as-synthesized SnS_2 and SnS_2/graphene were used directly for electrochemical characterization without any further heat treatment.

Material Characterization. To characterize the morphology of the samples, FE-SEM (S4700, Hitachi, Japan) and HR-TEM (TECNAI, Philips, Netherlands, 200 KeV) were employed. XRD analysis was performed using a Rigaku Rint 1000 (Japan) instrument with a Cu Kα radiation source. Raman spectra were recorded with a confocal microprobe Raman system (Lab Ram HR 800, Horiba,

DOI: 10.1021/acsami.7b11040
ACS Appl. Mater. Interfaces 2017, 9, 40187−40196

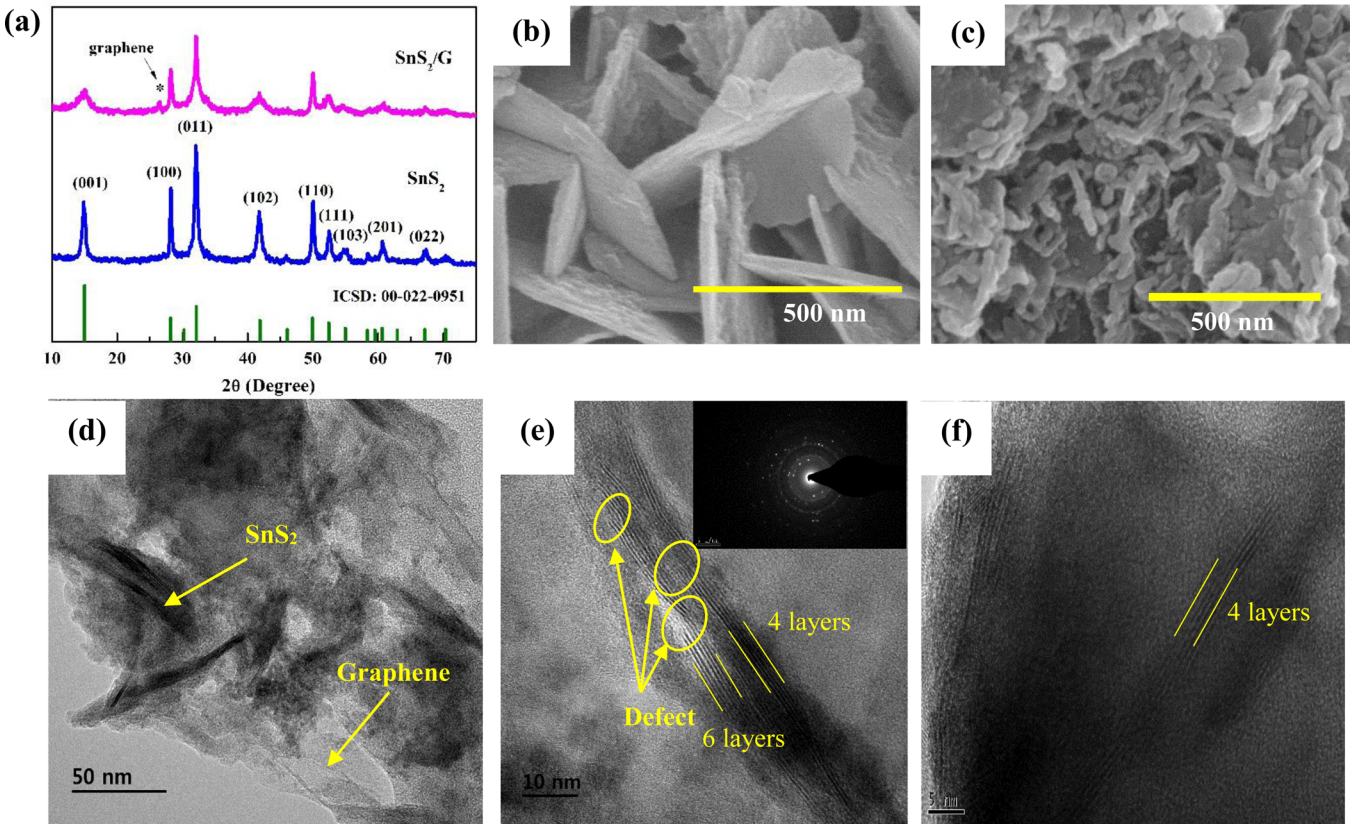

Figure 2. (a) XRD patterns of SnS_2 and SnS_2/G; SEM images of (b) SnS_2 and (c) SnS_2/G; and (d–f) TEM images of SnS_2/G.

Japan). The nitrogen adsorption/desorption isotherms were recorded by a Micromeritics ASAP 2010 surface area analyzer to characterize the BET surface area and porous texture. TGA (STA 1640, Stanton Redcroft Inc., UK) was performed at a heating rate of 5 °C min^{-1} under air to determine the graphene content.

Electrochemical Measurement. The electrochemical performance of both half-cells and full cells was evaluated using CR2032 coin cells. The electrodes used to examine the half-cell performance of SnS_2 had the following composition: 80% active material, 10% Ketjenblack (conductive carbon), and 10% poly(acrylic acid) binder. To fabricate the anodes, the electrode slurry was rolled over copper foil and then dried at 120 °C overnight in a vacuum oven. The typical mass loading of the anode was 1.5 mg cm^{-2}. Sodium foil is used as the counter electrode, and glass fiber separators were employed. Cyclic voltammetry and galvanostatic charge/discharge studies were performed using a Bio-Logic electrochemical workstation (SP-150, France) and a Won-A-Tech Battery tester (WBCS 3000, Korea), respectively. The discharge capacity and current density calculations in the half-cell studies of SnS_2 included the masses of both SnS_2 and graphene.

For the sodium full cells, SnS_2/G and an in-house-fabricated NVP are employed as the anode and cathode, respectively. The composition of the cathode is similar to that mentioned above, and the cathode slurry was coated on a stainless foil and then dried at 120 °C overnight in a vacuum oven. The typical cathode mass loading was ~3–3.5 mg cm^{-2}. Before full cell assembly, the SnS_2/G anode was cycled against sodium foil in the half-cell configuration a few times to eliminate the initial irreversible capacity loss (a common practice adapted by other studies).[10,13,16] The electrolyte consisted of $NaClO_4$ in 1:1 (v/v) ethylene carbonate:dimethyl carbonate. All the operations were performed inside an argon-filled glovebox. To obtain an appropriate cell balance, the negative-to-positive capacity ratio was set to approximately 1.2. In the full cell, the current density and capacity calculations considered only the mass of the cathode. The energy and power density calculations for the full cell are based on the combined mass of both the anode and cathode. NVP was synthesized by a sol–gel technique described in our previous report, and reduced GO served as the conductive network.[8] The electrochemical performance of NVP is given in Supporting Information (SI).

RESULTS AND DISCUSSION

Nanostructured few-layered SnS_2/G was synthesized directly through a one-pot microwave irradiation procedure without any additional calcination step. Briefly, when $SnCl_2$ was dissolved in a graphene oxide (GO) suspension, Sn^{2+} was adsorbed over the GO surface owing to strong electrostatic interactions with surface functionalities. Defect sites on the graphene sheets provided nucleation spots for the formation of SnS_2 crystals. During microwave irradiation, thiourea supplied an adequate sulfur source and atmosphere for the formation of SnS_2 crystals over the graphene layers. Microwave irradiation in the presence of the highly exfoliated graphene sheets synergistically inhibited the formation of large particles and facilitated the production of few-layered crystals.[27,30] The formation of SnS_2 crystals over graphene is illustrated in Figure 1.

The phase structures of the pristine SnS_2 (SnS_2) and SnS_2/G were confirmed by X-ray diffraction (XRD) measurements. The XRD patterns of SnS_2 and SnS_2/G in Figure 2a confirm that pure phases of the materials were obtained; the patterns can be readily assigned to hexagonal-type SnS_2. The XRD spectrum of SnS_2/G displays an additional peak at ~25.9° originating from the (002) plane of the graphene layer; the position of this peak indicates that the graphene was reduced by the microwave irradiation and thiourea.[20] The broadened and less intense (001) diffraction peak of SnS_2/G indicates the formation of unstacked and few-layered SnS_2 crystals.[19,31] The growth along the (001) plane of SnS_2 and agglomeration of SnS_2 layers were strongly disrupted by the presence of the graphene layers.[19,32]

DOI: 10.1021/acsami.7b11040
ACS Appl. Mater. Interfaces 2017, 9, 40187–40196

Field emission scanning electron microscopy (FE-SEM) images of SnS_2(Figures 2b and S1) show nanoplate morphology with a thickness of ~5 nm, where the nanoplates are aggregated and form a hierarchical spherical flower-like morphology. However, SnS_2/G shows densely packed and nonagglomerated SnS_2 particles over graphene sheets, where the particle agglomeration was strongly inhibited by the presence of the graphene sheets (Figure 2c). The elemental mapping of SnS_2/G (Figure S1c) shows the uniform distribution of Sn, S, and C elements. The transmission electron microscopy (TEM) image of SnS_2/G in Figure 2d further reveals that well-dispersed, few-layered SnS_2 was grown over the graphene sheets and shows good interconnection. The lattice fringes of high-resolution TEM (HR-TEM) images reveal an interlayer spacing of ~0.596 nm, which corresponds to the (001) plane of hexagonal SnS_2. The HR-TEM images further reveal that the number of stacked SnS_2 layers is as low as three (Figure 2e,f). Furthermore, few disorders and defects are observed in the exfoliated layered structure, so the material is favorable for the insertion of more sodium ions into the layered structure.[33−35] The transparency of the graphene in the TEM images indicates that only a few graphene layers are present. The corresponding selected area electron diffraction pattern shows clear concentric rings, indicating that the SnS_2/G is highly crystalline and can be well indexed to hexagonal-type SnS_2.[36]

The surface feature of GMMS is further investigated by XPS studies and given in Figure S2. The Sn 3d spectrum of SnS_2/G shows two peaks at ~487 and 495.5 eV, corresponding to the Sn $3d_{5/2}$ and Sn $3d_{3/2}$ photoelectron emission spectrum of tetravalent Sn. Furthermore, the deconvoluted C 1s spectrum shows the reduced intensity of oxygen containing functional groups, revealing that graphene layers exist in reduced nature. The Raman spectrum of SnS_2 and SnS_2/G in Figure 3a shows a strong peak at ~312 cm^{-1}, which is assigned to the first-order, in-plane vibrational A_{1g}mode of hexagonal-type SnS_2. The intensity of A_{1g} mode becomes much weaker due to phonon confinement, indicating a presence of a few-layered architecture in SnS_2/G, and this is in correlation with TEM analysis. Furthermore, the two characteristic bands of graphene, the G and D bands, are clearly visible at ~1326 and 1596 cm^{-1}, respectively.[37] The G band originates from vibrations in the graphitic sp^2 carbon atom planes, and the D band is ascribed to defects and disorders in the graphene layers. The calculated I_D/I_G intensity ratio is ~1.07, and the high value indicates the highly defective nature of the graphene sheets after microwave irradiation.[38] Additionally, a broad 2D band of graphene is also present at ~2700 cm^{-1}, indicating that the graphene sheets are predominantly a mixture of single-layer and few-layer nanosheets. However, pristine SnS_2 does not show G and D bands, indicating the absence of carbon. The results are in good agreement with the HR-TEM and XRD results. The well-exfoliated few-layered graphene could play a dual role by enhancing the electronic conductivity and immobilizing the SnS_2 particles by inhibiting particle detachment from the graphene sheets during high-volume-change reactions.[40]

The N_2 adsorption/desorption isotherms of SnS_2 and SnS_2/G are shown in Figure 3b and indicate the highly mesoporous nature of SnS_2/G. The Brunauer−Emmett−Teller (BET) surface area of SnS_2 is ~25 $m^2\ g^{-1}$; with the addition of graphene, it increases dramatically to ~80 $m^2\ g^{-1}$. SnS_2/G exhibits a type IV isotherm, and the major contribution to the surface area is that of the graphene sheets.[39] Further, like the graphene sheets, SnS_2 has a high concentration of mesopores,

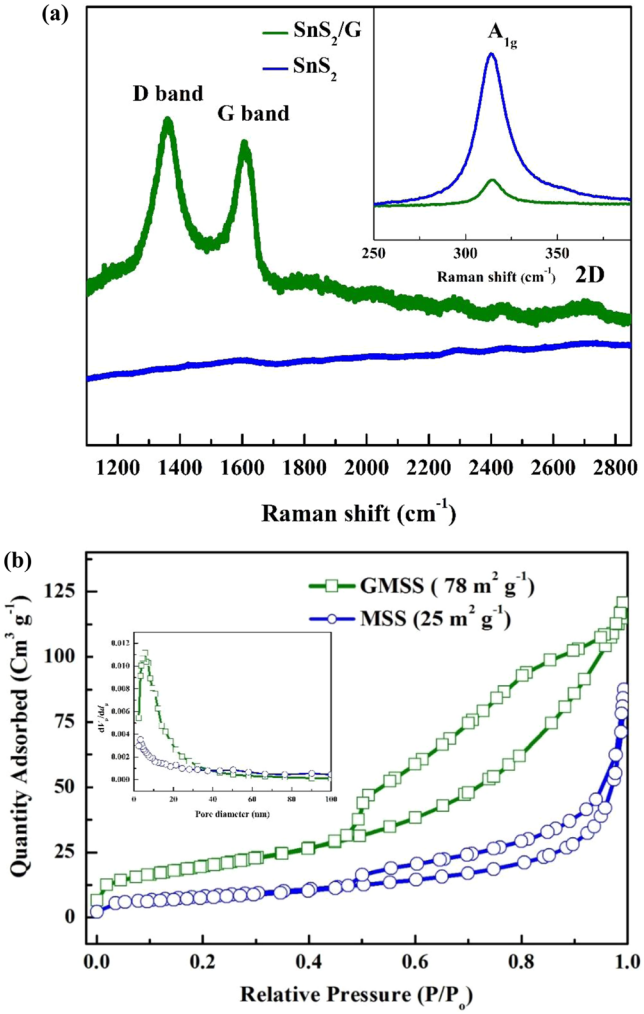

Figure 3. (a) Raman spectrum of SnS_2 and (b) nitrogen adsorption/desorption isotherms of SnS_2 and SnS_2/G.

as demonstrated by the Barrett−Joyner−Halenda plot (inset: Figure 3b). The presence of a large number of smaller mesopores contributes greatly to the short sodium diffusion path in the SnS_2 layers and also the ability to accommodate large volume changes during sodium storage, thereby affording high current density.[41] The weight percentage of graphene in SnS_2/G is quantitatively calculated to be ~13% from the thermogravimetric analysis (TGA) curves (Figure S3).

The highly favorable characteristics of SnS_2/G, including its ultrathin few-layered architecture, surface defects over the SnS_2 layers, highly electrically conductive graphene network, and short mesoporous sodium conducting channels, could synergistically shorten the sodium ion diffusion length and make it possible to store a large number of sodium ions in a very short time. The combination of the high surface area and few-layered architecture could greatly enhance the electrode−electrolyte interfacial area and reduce the interfacial resistance. This suggests that SnS_2/G could afford high energy and high power when it is applied in sodium full cells.

Figure 4a shows the initial charge/discharge curves of SnS_2/G at a current density of 100 mA g^{-1}. The first discharge and charge capacities of SnS_2/G were 950 and 702 mAh g^{-1}, respectively, corresponding to a Coulombic efficiency of ~75%. This low Coulombic efficiency and irreversible capacity loss in the first cycle are attributed to the formation of the solid−

DOI: 10.1021/acsami.7b11040
ACS Appl. Mater. Interfaces 2017, 9, 40187−40196

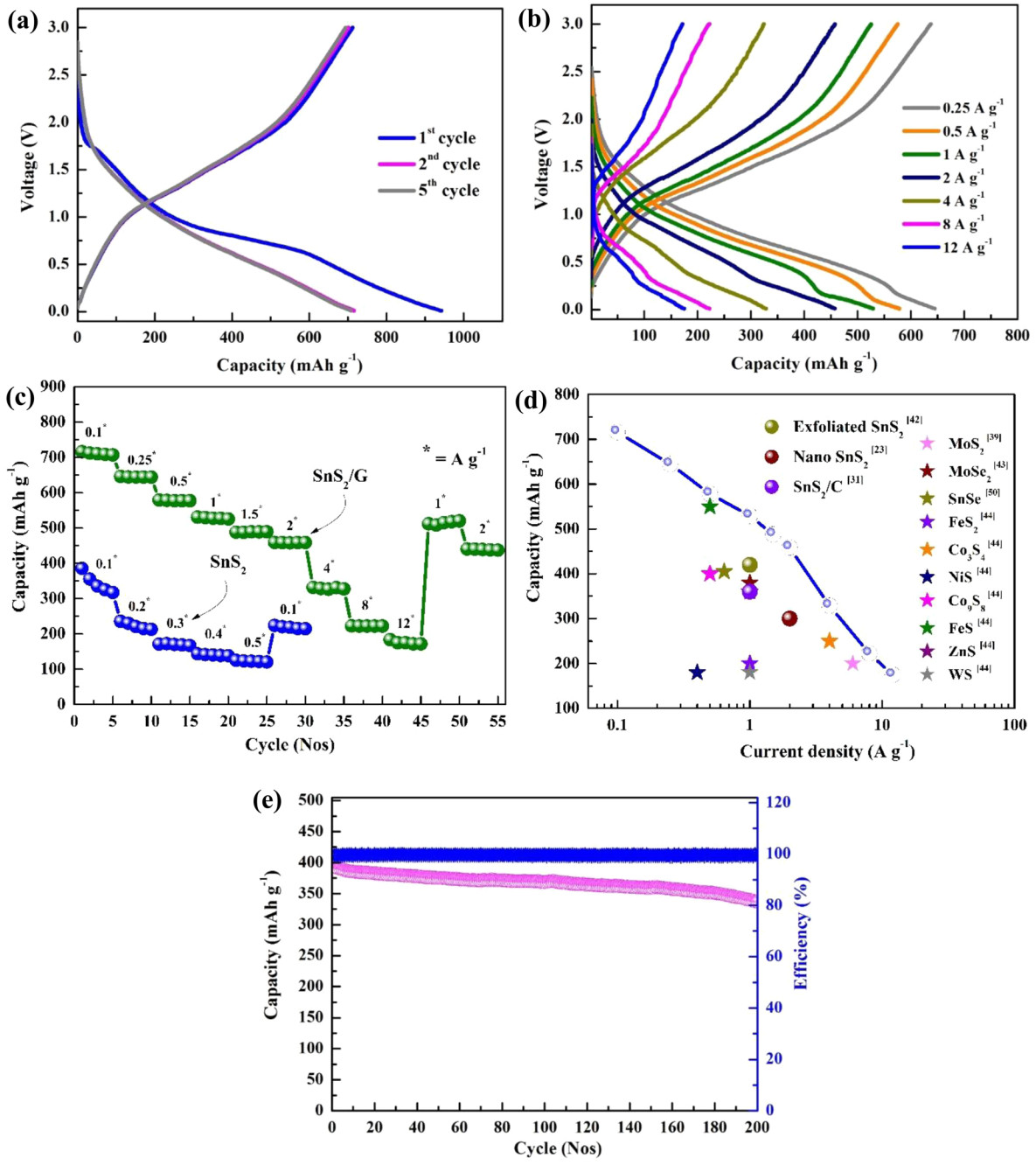

Figure 4. (a) Initial charge/discharge curves of SnS_2/G and (b) charge/discharge curves of SnS_2/G at different current densities; (c) rate performance of SnS_2/G and SnS_2; (d) cyclic stability of SnS_2/G at 2.5 A g^{-1}; and (e) performance comparison of SnS_2/G and previously reported anodes.

electrolyte interface at a lower voltage.[36,40] However, SnS_2/G showed excellent reversibility from the second cycle onward, with a Coulombic efficiency near ~99%, as demonstrated by the good overlap of the charge/discharge curves. A small plateau at ~1.7 V in the first discharge curve is attributed to the intercalation of Na ions into the (001) plane.[42] The key sodium ion charge storage occurs around 0.6 V and results primarily from conversion and alloying reactions involving Na−Sn and Na−S phase formation, which deliver high capacity. The discharge mechanism involves initial generation of amorphous Na_2S_2 and metallic Sn nanoparticles that further undergo the alloying reaction to form $Na_{15}S_4$. Upon charging, $Na_{15}S_4$ is dealloyed to form metallic Sn, which further reacts with Na_2S_2 to yield a SnS_2 phase between 1 and 1.5 V. For comparison, the sodium storage performance of bare SnS_2 was also tested.[17,42] Bare SnS_2 delivered a lower capacity than SnS_2/G and showed high polarization even under a low current rate (Figure S4). The low discharge capacity is attributed to poor electronic conductivity between the SnS_2 particles, which impedes the conversion kinetics for sodium storage. The poor electronic conductivity leads to high polarization and a high interfacial reaction energy during discharge in pristine SnS_2.[43] The obtained reversible specific capacity is much higher than that of metal oxide and carbonaceous anodes reported for SIBs.[18]

A superior rate capability is crucial in high-power anode materials for large-scale storage applications. SnS_2/G delivered

DOI: 10.1021/acsami.7b11040
ACS Appl. Mater. Interfaces 2017, 9, 40187−40196

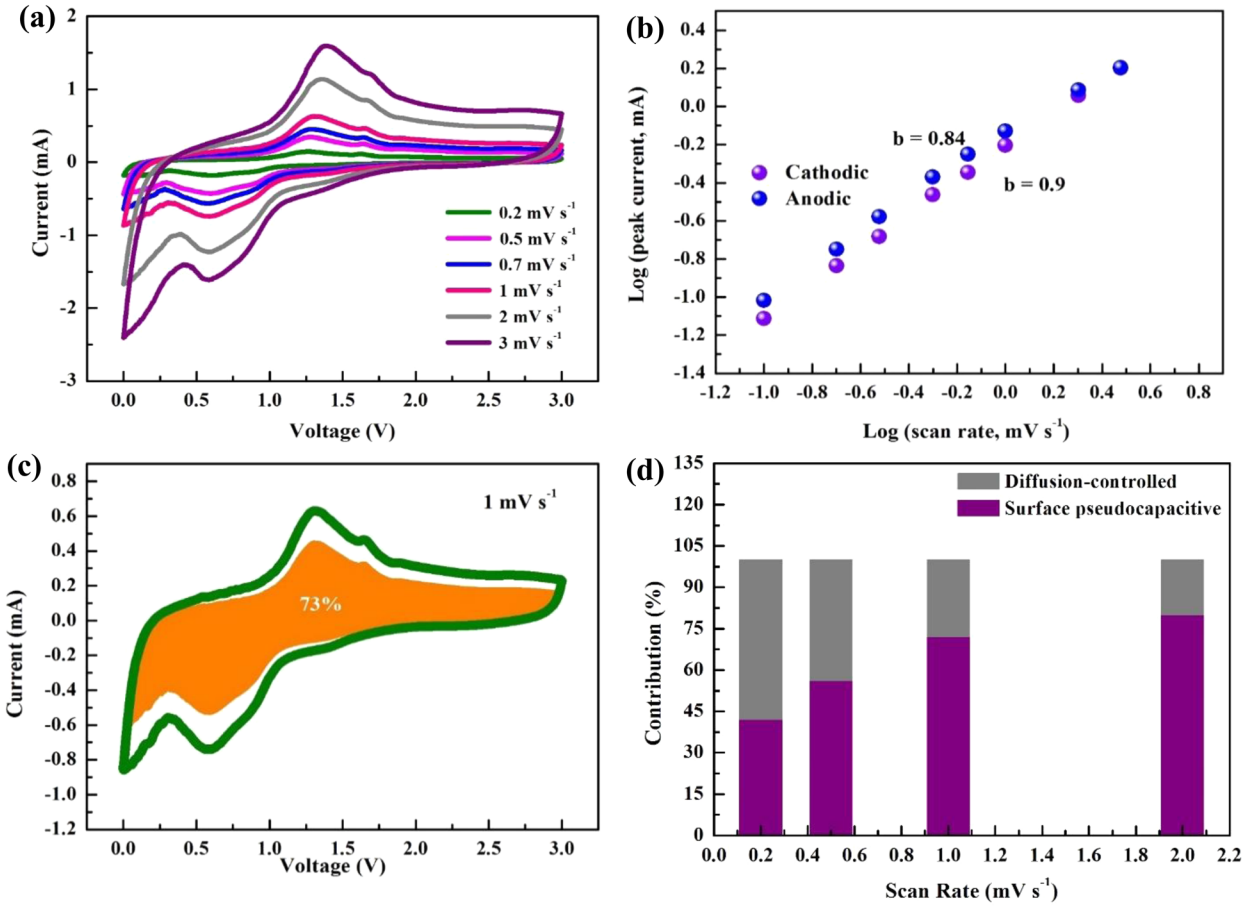

Figure 5. (a) CV curves of SnS_2/G at different scan rates; (b) current vs scan rate relationship for SnS_2/G; (c) pseudocapacitance contribution at 1 mV s^{-1}; and (d) charge storage contributions at different scan rates.

remarkable performance by retaining a capacity of ~647, 579, 531, 490, and 460 mAh g^{-1} at 0.25, 0.5, 1, 1.5, and 2 A g^{-1}, respectively. Even at a robust 12 A g^{-1}, where conversion is sluggish and alloy-type anodes fail to work, SnS_2/G retained a decent discharge capacity of ~172 mAh g^{-1}. A charge/discharge plateau is clearly visible even at this high current, indicating fast reaction kinetics. Furthermore, SnS_2/G displayed excellent capacity recovery, delivering over ~650 mAh g^{-1} when the rate current was brought back to 0.1 A g^{-1}. The discharge capacity is almost equal to the initial capacities, confirming the structural integrity of the SnS_2/G architecture, which enables it to withstand a harsh environment. In contrast, SnS_2 showed poor rate performance, delivering a discharge capacity of ~120 mAh g^{-1} at 0.5 A g^{-1} and inferior capacity recovery (Figure 4b,c). The capacity retention of SnS_2/G at a high current is superior to that of metal oxide and carbonaceous anodes. Figure 4d shows that the rate capability of the few-layered SnS_2/G is several times higher than that of previously reported analogous metal sulfides and metal selenides.[18,44,45] Note that the capacity and current density calculation includes the mass of both the active SnS_2 and graphene, whereas many earlier reports used only the mass of SnS_2 in the carbon matrix. Additionally, Table S1 compares the performance of microwave synthesized SnS_2/G with previously reported SnS_2 systems. This superior rate performance is expected to support the development of high-power SIBs. The high rate performance of SnS_2/G originates mainly from the well-dispersed, few-layered SnS_2 morphology, which provides a large number of reaction sites for sodium storage. Low polarization along with ultrafast charge transfer reactions enabled this superior rate performance. Additionally, the graphene sheets greatly enhance the sodium diffusion kinetics by providing short 2D electron-conducting channels. Furthermore, the few-layered SnS_2 and graphene sheets synergistically mitigate any mechanical stress and strain during high-current conditions. SnS_2 does not exhibit this behavior, so it does not provide the fast sodium storage kinetics. HR-TEM and SEM was employed to assess the structural stability of SnS_2/G after cycling. SEM images show that SnS_2 particles are well adhered to the graphene layer even after cycling. The HR-TEM images in Figure S5 confirm that the layered structure is well maintained with almost no change and is well preserved even after high-current conditions. The volume changes with sodiation/desodiation can easily accommodated by layered graphene sheets.

Durability at a high current rate is also crucial to practical application, and the long-term performance of SnS_2 anodes at high current rates has not yet been investigated. Figure 4e shows the long-term cyclic stability of SnS_2/G. At 2.5 A g^{-1}, SnS_2/G delivered a specific capacity of 394 mAh g^{-1} and retained a capacity of ~338 mAh g^{-1} after 150 cycles, corresponding to a retention of 86% with nearly 100% Coulombic efficiency. This material exhibited promising stability even at a high current density, indicating strong potential for its use in high-power sodium full cells. In contrast, SnS_2 exhibited poor cyclic stability, losing the ability to store sodium ions within a few cycles even at a low current (Figure

DOI: 10.1021/acsami.7b11040
ACS Appl. Mater. Interfaces 2017, 9, 40187−40196

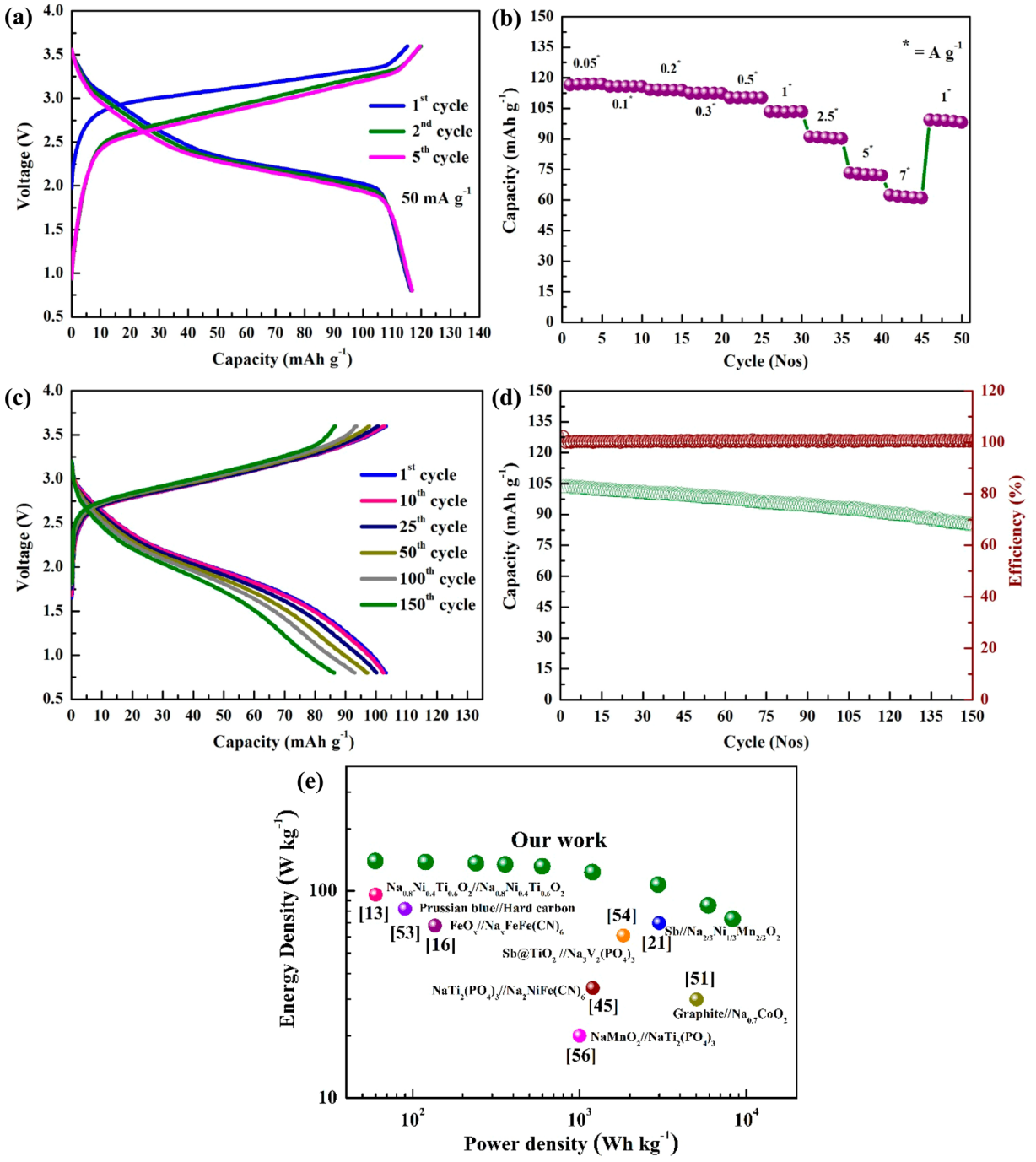

Figure 6. (a) First charge/discharge curves of SnS_2/G/NVP full cell; (b) rate performance of full cell; (c) cyclic stability of full cell at 1 A g^{-1}; (d) charge/discharge curves at 1 A g^{-1}; and (e) Ragone plot comparing energy and power output of full cell with previously reported values.

S6). Consequently, the effect of graphene content on SnS_2/G is also evaluated (Figure S7). The low quantity of graphene (7%) is not favorable for achieving a stable cycle performance as it is insufficient for accommodating SnS_2 particles and overcoming the volume change during sodiation/desodiation. While, a high quantity (21%) is not favorable for achieving a high capacity as a high quantity of graphene layers will block sodium movement.

To better understand the fast sodium storage kinetics of SnS_2/G, cyclic voltammetry (CV) tests were performed at various scan rates (Figure 5a). The CV curves display a sharp cathodic peak at ~0.6 V corresponding to the alloying and conversion reaction kinetics that form the $Na_{15}S_4$ phase. The broad anodic peak at ~1.2 V corresponds to reformation of the SnS_2 phase. As the scan rate increases, the shape of the CV curves is preserved well, indicating an extremely fast reaction.[42] The charge storage behavior can be evaluated in terms of the correlation between the scan rate and the measured output current in the CV curves, which can be obtained from the power law equation $i = a\nu^b$, where i is the output current (A), a and b are constants, and ν is the scan rate (mV s^{-1}). For diffusion-controlled processes, b is 0.5, whereas for surface-limited pseudocapacitive behavior, b is 1.[46] The output current in CV tests is directly proportional to the sweep rate according to the power law, and b is calculated to be ~0.9, implying that

DOI: 10.1021/acsami.7b11040
ACS Appl. Mater. Interfaces 2017, 9, 40187−40196

sodium charge storage in SnS_2/G is controlled mainly by surface pseudocapacitive reactions (Figure 5b). This explains the outstanding fast rate performance of SnS_2/G compared to conventional anodes based on sluggish diffusion-controlled storage mechanisms.[15,17,23,24]

Furthermore, the quantitative storage contributions in SnS_2/G can be evaluated from the relationship $i(V) = k_1\nu$ (capacitive) + $k_2\nu^{1/2}$ (diffusion-limited), where k_1 and k_2 are suitable constants obtained from linear plots of $\nu^{1/2}$ vs $i(V)\nu^{1/2}$ at a certain voltage. The pseudocapacitive current as a percentage of the total current at a fixed voltage can be quantitatively calculated by separating the current response (i) at the fixed voltage (Figure S8).[47] As a result, at 1 mV s^{-1}, the pseudocapacitive contribution to the total capacity is calculated to be 73%, as shown in Figure 5c,d. In addition, the fast pseudocapacitive contribution increases and the slow diffusion-limited intercalation contribution decreases with increasing scan rate. This clearly implies that few-layered defective SnS_2 nanosheets embedded in highly conductive graphene offer a large number of active sites for surface-induced pseudocapacitive sodium storage.

High-energy, high-power SIBs can be realized by using SnS_2/G in conjunction with a suitable high-performance and kinetically superior cathode. For the full SIB, we coupled SnS_2/G with an in-house-made NVP cathode material. The large three-dimensional open frameworks in NVP provide large channels for Na^+ ion movement, making it a sodium superionic conductor.[8,48] The high sodium ion conductivity and high chemical diffusion coefficient of NVP can provide relatively fast kinetics that could match well the fast sodium storage of SnS_2/G.[49,50]

The full cells were tested in the voltage range of 0.6−3.8 V. The initial charge/discharge curves of the SnS_2/G//NVP full cell are shown in Figure 6. A reversible capacity of 115 mAh g^{-1} was obtained in the first cycle at 0.05 A g^{-1} (based on the cathode mass) along with a high initial Coulombic efficiency of ∼99%, which approaches 100% starting in the second cycle (Figure 6a). The shape profile and specific capacity are well maintained throughout subsequent cycles, indicating highly reversible sodium ion storage in the full cell. The sodium full cell displays a high average potential of ∼2.4 V with a stable plateau. The storage mechanism in the full cell is as follows: (i) during charging, sodium ions are deintercalated from the NVP ($V^{3+/4+}$) and stored in the SnS_2/G by the alloying reaction, and (ii) during discharging, the sodium ions are intercalated back into the NVP from the SnS_2/G.[49]

Knowledge of the rate capability is essential for estimating the high-power behavior of a sodium full cell. The sodium full cell can cycle efficiently even at a high current rate of 7 A g^{-1} and retains ∼53% of its initial discharge capacity even when the current density increases by 140 times (Figure 6b). After the rate performance test, the full cell showed an exceptional capacity recovery to ∼100 mAh g^{-1} when the current density was returned to 1 A g^{-1}. This remarkable rate performance is greatly superior to that of lithium-ion-based energy storage systems. Figure 6c,d shows the long-term performance of the full cell, which showed a superior retention of 90% even after 150 cycles at 1 A g^{-1}. Nevertheless, at this high current density, the cell performed extremely well, with good retention, making it a prominent candidate for practical applications.

The Ragone plot in Figure 6d demonstrates the superiority of the full cell. The Ragone plot compares the energy and power output (based on the active mass of both electrodes) of the full cell with those of previously reported sodium full cells.[50,51] A high specific energy of ∼140 Wh kg^{-1} was delivered at 60 W kg^{-1}. A remarkable specific power of 8.3 kW kg^{-1} was achieved, along with a specific energy retention of 74 Wh kg^{-1}, which is competitive with high-power capacitors and is also higher than the values of previously reported sodium full cells.[21,50,52−58]

The exceptional performance of SnS_2/G originates mainly from the nanoscale, few-layered morphology of SnS_2, which exhibits nondestructive fast pseudocapacitive sodium storage. The highly exfoliated few-layered morphology provides abundant active sites for the pseudocapacitive reaction. The large number of mesopore channels originating from the graphene sheets effectively provides a short sodium ion diffusion path. The few-layered defective SnS_2 layers can accommodate a high volume change upon sodium storage and therefore maintain their structural integrity for longer cycling periods. Because of this structural stability, the 2D layered structure can exhibit greatly reduced interfacial resistance upon cycling.

CONCLUSION

Highly exfoliated nanoscale few-layered SnS_2 over graphene sheets was synthesized in a few minutes by microwave irradiation. The few-layered SnS_2 delivered outstanding performance with high capacity, ultrahigh rate capability, and excellent capacity recovery and stability when it was examined as an anode for SIBs. The highly mesoporous 2D few-layered SnS_2 crystals over graphene sheets provide fast pseudocapacitive sodium ion storage that enables better performance than low-capacity, low-power metal oxide and carbonaceous anodes. Furthermore, the high-performance SnS_2 demonstrated excellent output performance with high stability, a high initial Coulombic efficiency, a high energy of ∼140 Wh kg^{-1}, and a high power of 8.3 kWh kg^{-1} in a full-cell configuration; it shows strong potential for use in high-power energy storage devices with performance exceeding that of lithium ion batteries and capacitors. Our current research provides valuable insight into the development of high-capacity and high-rate sodium anodes toward realization of high-energy, high-power SIBs.

ASSOCIATED CONTENT

Supporting Information

The Supporting Information is available free of charge on the ACS Publications website at DOI: 10.1021/acsami.7b11040.

SEM image of SnS_2; SEM image of SnS_2/G; elemental mapping of SnS_2/G; XPS spectrum of SnS_2/G; TGA spectrum of SnS_2/G and SnS_2; CD curves of SnS_2 and SnS_2/G; TEM and SEM images of SnS_2/G after cycling; cyclic stability of SnS_2; cyclic stability of SnS_2/G with different graphene content; sweep rate dependence of output current at various potential ranges; half-cell performance of $Na_3V_2(PO_4)_3$ cathode; table comparing the performance of several reported SnS_2 anodes for sodium ion batteries (PDF)

AUTHOR INFORMATION

Corresponding Author

*Tel. & Fax: +82 62 530 1904; E-mail: leeys@chonnam.ac.kr (Y.-S.L)

ORCID

Hari Vignesh Ramasamy: 0000-0002-8241-2441

DOI: 10.1021/acsami.7b11040
ACS Appl. Mater. Interfaces 2017, 9, 40187−40196

Yun-Sung Lee: 0000-0002-6676-2871

Notes

The authors declare no competing financial interest.

■ ACKNOWLEDGMENTS

This work was supported by the National Research Foundation of Korea (NRF) grant funded by the Korea government (Ministry of Science, ICT & Future Planning) (No. 2016R1A4A1012224).

■ REFERENCES

(1) Armand, M.; Tarascon, J. M. Building Better Batteries. *Nature* **2008**, *451*, 652−657.
(2) Kang, K.; Meng, Y. S.; Bréger, J.; Grey, C. P.; Ceder, G. Electrodes with High Power and High Capacity for Rechargeable Lithium Batteries. *Science* **2006**, *311*, 977−980.
(3) Kim, H.; Kim, H.; Ding, Z.; Lee, M. H.; Lim, K.; Yoon, G.; Kang, K. Recent Progress in Electrode Materials for Sodium-Ion Batteries. *Adv. Energy Mater.* **2016**, *6*, 1600943.
(4) Tarascon, J. M.; Armand, M. Issues and Challenges Facing Rechargeable Lithium Batteries. *Nature* **2001**, *414*, 359−367.
(5) Kim, S.-W.; Seo, D.-H.; Ma, X.; Ceder, G.; Kang, K. Electrode Materials for Rechargeable Sodium-Ion Batteries: Potential Alternatives to Current Lithium-Ion Batteries. *Adv. Energy Mater.* **2012**, *2*, 710−721.
(6) Wu, C.; Kopold, P.; Ding, Y.-L.; van Aken, P. A.; Maier, J.; Yu, Y. Synthesizing Porous NaTi2(PO4)3 Nanoparticles Embedded in 3D Graphene Networks for High-Rate and Long Cycle-Life Sodium Electrodes. *ACS Nano* **2015**, *9*, 6610−6618.
(7) Thangavel, R.; Kaliyappan, K.; Kim, D.-U.; Sun, X.; Lee, Y.-S. All-Organic Sodium Hybrid Capacitor: A New, High-Energy, High-Power Energy Storage System Bridging Batteries and Capacitors. *Chem. Mater.* **2017**, *29*, 7122−7130.
(8) Thangavel, R.; Kaliyappan, K.; Kang, K.; Sun, X.; Lee, Y.-S. Going Beyond Lithium Hybrid Capacitors: Proposing a New High-Performing Sodium Hybrid Capacitor System for Next-Generation Hybrid Vehicles Made with Bio-Inspired Activated Carbon. *Adv. Energy Mater.* **2016**, *6*, 1502199.
(9) Liu, Y.; Zhang, N.; Jiao, L.; Chen, J. Tin Nanodots Encapsulated in Porous Nitrogen-Doped Carbon Nanofibers as a Free-Standing Anode for Advanced Sodium-Ion Batteries. *Adv. Mater.* **2015**, *27*, 6702−6707.
(10) Liu, Y.; Fan, L.-Z.; Jiao, L. Graphene Highly Scattered in Porous Carbon Nanofibers: A Binder-Free and High-Performance Anode for Sodium-Ion Batteries. *J. Mater. Chem. A* **2017**, *5*, 1698−1705.
(11) Zhu, H.; Jia, Z.; Chen, Y.; Weadock, N.; Wan, J.; Vaaland, O.; Han, X.; Li, T.; Hu, L. Tin Anode for Sodium-Ion Batteries Using Natural Wood Fiber as a Mechanical Buffer and Electrolyte Reservoir. *Nano Lett.* **2013**, *13*, 3093−3100.
(12) Hou, H.; Qiu, X.; Wei, W.; Zhang, Y.; Ji, X. Carbon Anode Materials for Advanced Sodium-Ion Batteries. *Adv. Energy Mater.* **2017**, 1602898.
(13) Guo, S.; Yu, H.; Liu, P.; Ren, Y.; Zhang, T.; Chen, M.; Ishida, M.; Zhou, H. High-Performance Symmetric Sodium-Ion Batteries Using a New, Bipolar O3-Type Material, Na0.8Ni0.4Ti0.6O2. *Energy Environ. Sci.* **2015**, *8*, 1237−1244.
(14) Ramasamy, H. V.; Kaliyappan, K.; Thangavel, R.; Aravindan, V.; Kang, K.; Sun, X.; Lee, Y.-S.; Kim, D. U.; Park, Y. Cu-Doped P2-Na0.5Ni0.33Mn0.67O2 Encapsulated with MgO as Novel High Voltage Cathode with Enhanced Na-Storage Properties. *J. Mater. Chem. A* **2017**, *5*, 8408−841.
(15) Liu, Y.; Zhang, N.; Yu, C.; Jiao, L.; Chen, J. MnFe2O4@C Nanofibers as High-Performance Anode for Sodium-Ion Batteries. *Nano Lett.* **2016**, *16*, 3321−3328.
(16) Ye, H.; Wang, Y.; Zhao, F.; Huang, W.; Han, N.; Zhou, J.; Zeng, M.; Li, Y. Iron-Based Sodium-Ion Full Batteries. *J. Mater. Chem. A* **2016**, *4*, 1754−1761.
(17) Chao, D.; Liang, P.; Chen, Z.; Bai, L.; Shen, H.; Liu, X.; Xia, X.; Zhao, Y.; Savilov, S. V.; Lin, J.; Shen, Z. X. Pseudocapacitive Na-Ion Storage Boosts High Rate and Areal Capacity of Self-Branched 2D Layered Metal Chalcogenide Nanoarrays. *ACS Nano* **2016**, *10*, 10211−10219.
(18) Zhang, Y.; Zhu, P.; Huang, L.; Xie, J.; Zhang, S.; Cao, G.; Zhao, X. Few-Layered SnS2 on Few-Layered Reduced Graphene Oxide as Na-Ion Battery Anode with Ultralong Cycle Life and Superior Rate Capability. *Adv. Funct. Mater.* **2015**, *25*, 481−489.
(19) Kang, J.-G.; Lee, G.-H.; Park, K.-S.; Kim, S.-O.; Lee, S.; Kim, D.-W.; Park, J.-G. Three-Dimensional Hierarchical Self-Supported Multi-Walled Carbon Nanotubes/Tin(IV) Disulfide Nanosheets Heterostructure Electrodes for High Power Li Ion Batteries. *J. Mater. Chem.* **2012**, *22*, 9330−9337.
(20) Jiang, Y.; Wei, M.; Feng, J.; Ma, Y.; Xiong, S. Enhancing the Cycling Stability of Na-Ion Batteries by Bonding SnS2 Ultrafine Nanocrystals on Amino-Functionalized Graphene Hybrid Nanosheets. *Energy Environ. Sci.* **2016**, *9*, 1430−1438.
(21) Liang, L.; Xu, Y.; Wang, C.; Wen, L.; Fang, Y.; Mi, Y.; Zhou, M.; Zhao, H.; Lei, Y. Large-Scale Highly Ordered Sb Nanorod Array Anodes with High Capacity and Rate Capability for Sodium-Ion Batteries. *Energy Environ. Sci.* **2015**, *8*, 2954−2962.
(22) Longoni, G.; Pena Cabrera, R. L.; Polizzi, S.; D'Arienzo, M.; Mari, C. M.; Cui, Y.; Ruffo, R. Shape-Controlled TiO2 Nanocrystals for Na-Ion Battery Electrodes: The Role of Different Exposed Crystal Facets on the Electrochemical Properties. *Nano Lett.* **2017**, *17*, 992−1000.
(23) Prikhodchenko, P. V.; Yu, D. Y. W.; Batabyal, S. K.; Uvarov, V.; Gun, J.; Sladkevich, S.; Mikhaylov, A. A.; Medvedev, A. G.; Lev, O. Nanocrystalline Tin Disulfide Coating of Reduced Graphene Oxide Produced by The Peroxostannate Deposition Route for Sodium Ion Battery Anodes. *J. Mater. Chem. A* **2014**, *2*, 8431−8437.
(24) Chao, D.; Zhu, C.; Yang, P.; Xia, X.; Liu, J.; Wang, J.; Fan, X.; Savilov, S. V.; Lin, J.; Fan, H. J.; Shen, Z. X. Array of Nanosheets Render Ultrafast and High-Capacity Na-Ion Storage by Tunable Pseudocapacitance. *Nat. Commun.* **2016**, *7*, 12122.
(25) Gao, M.-R.; Xu, Y.-F.; Jiang, J.; Yu, S.-H. Nanostructured Metal Chalcogenides: Synthesis, Modification, and Applications in Energy Conversion and Storage Devices. *Chem. Soc. Rev.* **2013**, *42*, 2986−3017.
(26) Chen, D.; Chen, W.; Ma, L.; Ji, G.; Chang, K.; Lee, J. Y. Graphene-Like Layered Metal Dichalcogenide/Graphene Composites: Synthesis and Applications in Energy Storage and Conversion. *Mater. Today* **2014**, *17*, 184−193.
(27) Amaresh, S.; Karthikeyan, K.; Jang, I. C.; Lee, Y. S. Single-Step Microwave Mediated Synthesis of the CoS2 Anode Material for High Rate Hybrid Supercapacitors. *J. Mater. Chem. A* **2014**, *2*, 11099−11106.
(28) Bilecka, I.; Niederberger, M. Microwave Chemistry for Inorganic Nanomaterials Synthesis. *Nanoscale* **2010**, *2*, 1358−1374.
(29) Rui, X.; Tan, H.; Yan, Q. Nanostructured Metal Sulfides for Energy Storage. *Nanoscale* **2014**, *6*, 9889−9924.
(30) Zhu, Y.-J.; Chen, F. Microwave-Assisted Preparation of Inorganic Nanostructures in Liquid Phase. *Chem. Rev.* **2014**, *114*, 6462−6555.
(31) Wang, J.; Luo, C.; Mao, J.; Zhu, Y.; Fan, X.; Gao, T.; Mignerey, A. C.; Wang, C. Solid-State Fabrication of SnS2/C Nanospheres for High-Performance Sodium Ion Battery Anode. *ACS Appl. Mater. Interfaces* **2015**, *7*, 11476−11481.
(32) Liu, Y.; Kang, H.; Jiao, L.; Chen, C.; Cao, K.; Wang, Y.; Yuan, H. Exfoliated-SnS2 Restacked on Graphene as a High-Capacity, High-Rate, and Long-Cycle Life Anode for Sodium Ion Batteries. *Nanoscale* **2015**, *7*, 1325−1332.
(33) Sahu, T. S.; Mitra, S. Exfoliated MoS2 Sheets and Reduced Graphene Oxide-An Excellent and Fast Anode for Sodium-ion Battery. *Sci. Rep.* [Online] **2015**, *5*.10.1038/srep12571
(34) Sun, X.; Wang, Z.; Fu, Y. Q. Defect-Mediated Lithium Adsorption and Diffusion on Monolayer Molybdenum Disulfide. *Sci. Rep.* [Online] **2016**, *5*.10.1038/srep18712

DOI: 10.1021/acsami.7b11040
ACS Appl. Mater. Interfaces 2017, 9, 40187−40196

(35) David, L.; Bhandavat, R.; Singh, G. MoS2/Graphene Composite Paper for Sodium-Ion Battery Electrodes. *ACS Nano* **2014**, *8*, 1759−1770.
(36) Zhou, T.; Pang, W. K.; Zhang, C.; Yang, J.; Chen, Z.; Liu, H. K.; Guo, Z. Enhanced Sodium-Ion Battery Performance by Structural Phase Transition from Two-Dimensional Hexagonal-SnS2 to Orthorhombic-SnS. *ACS Nano* **2014**, *8*, 8323−8333.
(37) Liu, Y.; Zhao, Y.; Jiao, L.; Chen, J. A Graphene-Like MoS2/Graphene Nanocomposite as a High performance Anode for Lithium Ion Batteries. *J. Mater. Chem. A* **2014**, *2*, 13109−13115.
(38) Kudin, K. N.; Ozbas, B.; Schniepp, H. C.; Prud'homme, R. K.; Aksay, I. A.; Car, R. Raman Spectra of Graphite Oxide and Functionalized Graphene Sheets. *Nano Lett.* **2008**, *8*, 36−41.
(39) Rajendiran, S.; Park, K.; Lee, K.; Yoon, S. Ionic-Liquid-Based Heterogeneous Covalent Triazine Framework Cobalt Catalyst for the Direct Synthesis of Methyl 3-Hydroxybutyrate from Propylene Oxide. *Inorg. Chem.* **2017**, *56*, 7270−7277.
(40) Sun, W.; Rui, X.; Yang, D.; Sun, Z.; Li, B.; Zhang, W.; Zong, Y.; Madhavi, S.; Dou, S.; Yan, Q. Two-Dimensional Tin Disulfide Nanosheets for Enhanced Sodium Storage. *ACS Nano* **2015**, *9*, 11371−11381.
(41) Liu, Y.; Zhang, N.; Jiao, L.; Tao, Z.; Chen, J. Ultrasmall Sn Nanoparticles Embedded in Carbon as High-Performance Anode for Sodium-Ion Batteries. *Adv. Funct. Mater.* **2015**, *25*, 214−220.
(42) Ma, C.; Xu, J.; Alvarado, J.; Qu, B.; Somerville, J.; Lee, J. Y.; Meng, Y. S. Investigating the Energy Storage Mechanism of SnS2-rGO Composite Anode for Advanced Na-Ion Batteries. *Chem. Mater.* **2015**, *27*, 5633−5640.
(43) Xie, D.; Tang, W.; Wang, Y.; Xia, X.; Zhong, Y.; Zhou, D.; Wang, D.; Wang, X.; Tu, J. Facile Fabrication of Integrated Three-Dimensional C-MoSe2/Reduced Graphene Oxide Composite with Enhanced Performance for Sodium Storage. *Nano Res.* **2016**, *9*, 1618−1629.
(44) Xiao, Y.; Lee, S. H.; Sun, Y.-K. The Application of Metal Sulfides in Sodium Ion Batteries. *Adv. Energy Mater.* **2017**, *7*, 1601329.
(45) Wu, X.; Cao, Y.; Ai, X.; Qian, J.; Yang, H. A Low-Cost and Environmentally Benign Aqueous Rechargeable Sodium-Ion Battery Based on NaTi2(PO4)3−Na2NiFe(CN)6 Intercalation Chemistry. *Electrochem. Commun.* **2013**, *31*, 145−148.
(46) Huang, S.; Zhang, L.; Lu, X.; Liu, L.; Liu, L.; Sun, X.; Yin, Y.; Oswald, S.; Zou, Z.; Ding, F.; Schmidt, O. G. Tunable Pseudocapacitance in 3D TiO2−δ Nanomembranes Enabling Superior Lithium Storage Performance. *ACS Nano* **2017**, *11*, 821−830.
(47) Wu, Y.; Liu, X.; Yang, Z.; Gu, L.; Yu, Y. Nitrogen-Doped Ordered Mesoporous Anatase TiO2 Nanofibers as Anode Materials for High Performance Sodium-Ion Batteries. *Small* **2016**, *12*, 3522−3529.
(48) Thangavel, R.; Moorthy, B.; Kim, D. K.; Lee, Y.-S. Pushing the Energy Output and Cyclability of Sodium Hybrid Capacitors at High Power to New Limits. *Adv. Energy Mater.* **2017**, *7*, 1602654.
(49) Jian, Z.; Hu, Y.-S.; Ji, X.; Chen, W. NASICON-Structured Materials for Energy Storage. *Adv. Mater.* **2017**, *29*, 1601925.
(50) Yuan, S.; Zhu, Y.-H.; Li, W.; Wang, S.; Xu, D.; Li, L.; Zhang, Y.; Zhang, X.-B. Surfactant-Free Aqueous Synthesis of Pure Single-Crystalline SnSe Nanosheet Clusters as Anode for High Energy- and Power-Density Sodium-Ion Batteries. *Adv. Mater.* **2017**, *29*, 1602469.
(51) Hasa, I.; Dou, X.; Buchholz, D.; Shao-Horn, Y.; Hassoun, J.; Passerini, S.; Scrosati, B. A Sodium-Ion Battery Exploiting Layered Oxide Cathode, Graphite Anode and Glyme-Based Electrolyte. *J. Power Sources* **2016**, *310*, 26−31.
(52) Ding, J.; Wang, H.; Li, Z.; Cui, K.; Karpuzov, D.; Tan, X.; Kohandehghan, A.; Mitlin, D. Peanut Shell Hybrid Sodium Ion Capacitor with Extreme Energy-Power Rivals Lithium ion Capacitors. *Energy Environ. Sci.* **2015**, *8*, 941−955.
(53) Yang, D.; Xu, J.; Liao, X.-Z.; He, Y.-S.; Liu, H.; Ma, Z.-F. Structure Optimization of Prussian Blue Analogue Cathode Materials for Advanced Sodium Ion Batteries. *Chem. Commun.* **2014**, *50*, 13377−13380.
(54) Wang, N.; Bai, Z.; Qian, Y.; Yang, J. Double-Walled Sb@TiO2−x Nanotubes as a Superior High-Rate and Ultralong-Lifespan Anode Material for Na-Ion and Li-Ion Batteries. *Adv. Mater.* **2016**, *28*, 4126−4133.
(55) Zhu, C.; Kopold, P.; van Aken, P. A.; Maier, J.; Yu, Y. High Power−High Energy Sodium Battery Based on Threefold Interpenetrating Network. *Adv. Mater.* **2016**, *28*, 2409−2416.
(56) Hou, Z.; Li, X.; Liang, J.; Zhu, Y.; Qian, Y. An Aqueous Rechargeable Sodium Ion Battery Based on a NaMnO2-NaTi2(PO4)3 Hybrid System for Stationary Energy Storage. *J. Mater. Chem. A* **2015**, *3*, 1400−1404.
(57) Rani, J. R.; Thangavel, R.; Oh, S.-I.; Woo, J. M.; Chandra Das, N.; Kim, S.-Y.; Lee, Y.-S.; Jang, J.-H. High Volumetric Energy Density Hybrid Supercapacitors Based on Reduced Graphene Oxide Scrolls. *ACS Appl. Mater. Interfaces* **2017**, *9*, 22398−22407.
(58) Thangavel, R.; Kaliyappan, K.; Ramasamy, H. V.; Sun, X.; Lee, Y.-S. Engineering the Pores of Biomass-Derived Carbon: Insights for Achieving Ultrahigh Stability at High Power in High-Energy Supercapacitors. *ChemSusChem* **2017**, *10*, 2805−2815.

DOI: 10.1021/acsami.7b11040
ACS Appl. Mater. Interfaces 2017, 9, 40187−40196